




Article

Gurzhiite, $\text{Al}(\text{UO}_2)(\text{SO}_4)_2\text{F}\cdot 10\text{H}_2\text{O}$, a new uranyl sulfate mineral with a chain structure from the Bykogorskoe deposit, Northern Caucasus, Russia

Anatoly V. Kasatkin^{1*} , Jakub Plášil², Nikita V. Chukanov³, Radek Škoda⁴, Fabrizio Nestola⁵, Atali A. Agakhanov¹ and Dmitry I. Belakovskiy¹

¹Fersman Mineralogical Museum of the Russian Academy of Sciences, Leninsky Prospekt 18-2, 119071 Moscow, Russia; ²Institute of Physics of the CAS, Na Slovance 1999/2, 18221 Praha 8, Czech Republic; ³Institute of Problems of Chemical Physics of the Russian Academy of Sciences, 142432 Chernogolovka, Moscow region, Russia; ⁴Department of Geological Sciences, Faculty of Science, Masaryk University, Kotlářská 2, 611 37, Brno, Czech Republic; and ⁵Dipartimento di Geoscienze, Università di Padova, Via Gradenigo 6, I-35131, Padova, Italy

Abstract

Gurzhiite, ideally $\text{Al}(\text{UO}_2)(\text{SO}_4)_2\text{F}\cdot 10\text{H}_2\text{O}$, is a new uranyl sulfate mineral from the Bykogorskoe U deposit, Northern Caucasus, Russia. It occurs as fine-grained aggregates forming veinlets up to 50 cm long in cracks of the brecciated rock. Gurzhiite aggregates are composed of small bladed crystals up to 0.1 mm across. Associated minerals include khademite and quartz. Gurzhiite is pale yellow in crystals, lemon yellow in aggregates, transparent with a vitreous lustre and a white streak. It is brittle and has an irregular fracture. Cleavage is good on {001}. The new mineral exhibits a bright yellow–green fluorescence under both longwave and shortwave UV radiation. Mohs hardness is ~ 2 . $D_{\text{meas}} = 2.52(3)$ g/cm³ and $D_{\text{calc}} = 2.605$ g/cm³. The mineral is biaxial (–) with $\alpha = 1.528(3)$, $\beta = 1.538(2)$, $\gamma = 1.544(3)$ (589 nm); $2V_{\text{meas}} = 80(10)^\circ$ and $2V_{\text{calc}} = 75.1^\circ$. The empirical formula calculated on the basis of 21(O + F) atoms per formula unit (apfu) is $\text{Al}_{0.92}\text{Zn}_{0.05}\text{Fe}_{0.03}^{3+}\text{Na}_{0.03}\text{U}_{0.95}\text{S}_{2.00}\text{O}_{9.85}\text{F}_{0.99}\cdot 10.16\text{H}_2\text{O}$. Gurzhiite is triclinic, with space group $P\bar{1}$, $a = 7.193(2)$, $b = 11.760(2)$, $c = 11.792(2)$ Å, $\alpha = 67.20(3)$, $\beta = 107.76(3)$, $\gamma = 89.99(3)^\circ$, $V = 867.7(4)$ Å³ and $Z = 2$. The five strongest lines of the powder X-ray diffraction pattern [d , Å (I , %)(hkl)] are: 10.24(100)(001); 5.40(14)($\bar{1}\bar{1}1$); 5.11(54)(002); 3.405(11)($\bar{2}11$); and 3.065(11)($\bar{1}\bar{1}3$). The crystal structure of gurzhiite is based upon uranyl sulfate chains of the same type as in bobcookite and svornostite. Between the chains are two types of Al-octahedra – $\text{Al}(\text{H}_2\text{O})_6$ and $\text{Al}_2\text{F}_2(\text{H}_2\text{O})_4$. The entire structure stability is maintained by a complex network of H bonds. The new mineral honours Russian mineralogist and crystallographer Dr. Vladislav V. Gurzhiy in recognition for his contributions to uranium mineralogy and crystallography.

Keywords: gurzhiite, new mineral, uranyl sulfate, chain crystal structure, Bykogorskoe deposit, Northern Caucasus

(Received 10 January 2022; accepted 27 March 2022; Accepted Manuscript published online: 12 May 2022; Associate Editor: Daniel Atencio)

Introduction

Naturally occurring uranyl sulfate minerals are common in oxidised parts of uranium deposits worldwide. They form due to supergene processes, such as oxidation and hydration of primary uranium minerals, mainly uraninite, and their interaction with acid solutions derived from the decomposition of primary sulfides, such as pyrite, chalcopyrite or sphalerite. The alteration of primary uranium ores under low-pH conditions generates highly mobile acid solutions, containing dissolved UO_2^{2+} as $\text{UO}_2\text{--SO}_4$ aqueous complexes, which yields a considerable environmental impact, especially around the old mining sites (Krivovichev and Plášil, 2013; Plášil, 2014; Gurzhiy and Plášil, 2019). On the other hand, uranyl sulfates represent one of the most structurally and chemically complex families of naturally occurring U^{6+}

phases. To date, 57 uranyl sulfate minerals are known, almost two thirds (37 mineral species) of which were described during the last ten years, thanks to impressive finds at several old mines in Red Canyon, Utah, USA and Jáchymov, Czech Republic. Most of these species represent new structure types. Their dimensional and topological diversity and complexity were recently reviewed by Gurzhiy and Plášil (2019).

Herein, we describe another uranyl sulfate mineral with a novel structure that we named gurzhiite (pronouncing: gur zhi ait; cyrilic – гуржиит) in honour of Russian mineralogist and crystallographer Dr. Vladislav Vladimirovich Gurzhiy (born 17.12.1985), Associate Professor at the Department of Crystallography, and the Chairman of the Scientific Committee at the Institute of Earth Sciences, Saint-Petersburg State University. Dr. Gurzhiy is one of the leading Russian scientists in uranium mineralogy and crystallography. To date, he is the author and co-author of 47 publications focused on the crystal chemistry and structural complexity of uranium-bearing minerals and synthetic compounds (see, e.g. Gurzhiy *et al.*, 2016, 2018, 2019, 2020, 2021; Gurzhiy and Plášil, 2019 *et c.*).

*Author for correspondence: Anatoly V. Kasatkin, Email: anatoly.kasatkin@gmail.com

Cite this article: Kasatkin A.V., Plášil J., Chukanov N.V., Škoda R., Nestola F., Agakhanov A.A. and Belakovskiy D.I. (2022) Gurzhiite, $\text{Al}(\text{UO}_2)(\text{SO}_4)_2\text{F}\cdot 10\text{H}_2\text{O}$, a new uranyl sulfate mineral with a chain structure from the Bykogorskoe deposit, Northern Caucasus, Russia. *Mineralogical Magazine* 86, 412–421. <https://doi.org/10.1180/mgm.2022.34>

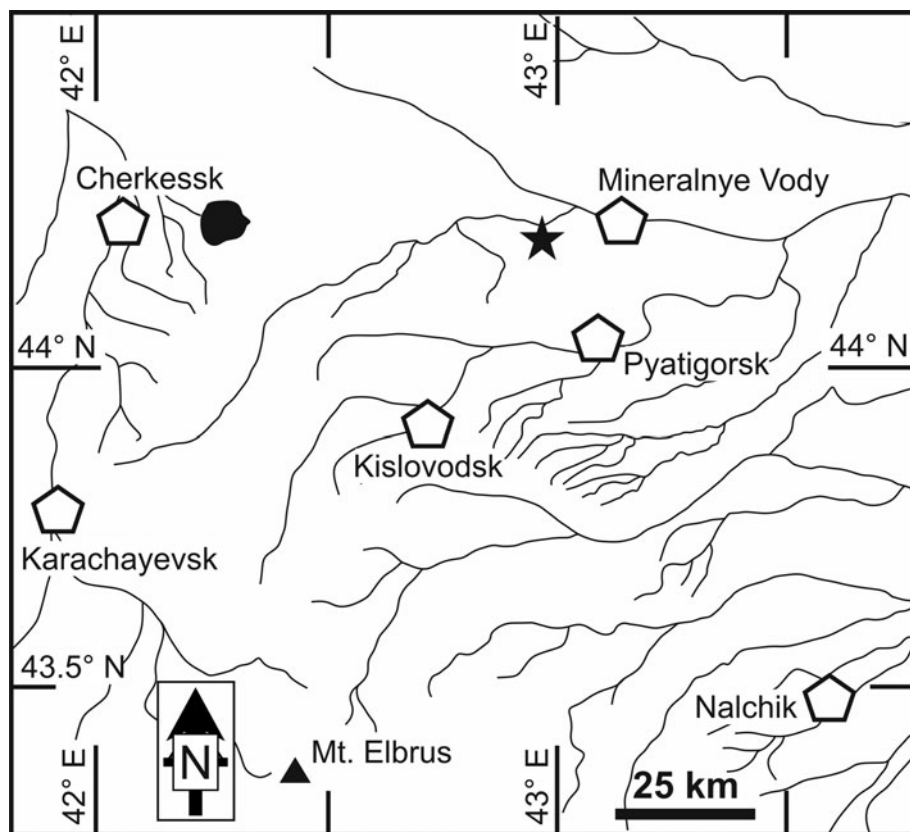


Fig. 1. Geographical position of Bykogorskoe U deposit (black star). Key: black lines and shaded areas = rivers and lakes; pentagon = city; triangle = Mt Elbrus.

The new mineral and its name (symbol Grz) have been approved by the Commission on New Minerals, Nomenclature and Classification of the International Mineralogical Association (IMA2021-086; Kasatkin *et al.*, 2022). The holotype specimen is deposited in the collections of the Fersman Mineralogical Museum of the Russian Academy of Sciences, Moscow, Russia, with the registration number 5756/1.

Occurrence and mineral association

The specimen that served as holotype was first discovered by Dmitry N. Tsebro in 2016. Additional material was also collected by him in 2019–2021. All the samples come from the 495 m level of the underground Mine #2, Bykogorskoe U deposit, Byk Mountain, Stavropol Krai, Northern Caucasus, Russia (44°11′05.4″N, 42°57′31.5″E) (Figs 1 and 2).

The Bykogorskoe U deposit is confined to the hypabyssal intrusion of granite-porphry (beshtaunites) that compose the dome-shaped uplift of Byk Mountain. The intrusion is surrounded by clayey and marly sedimentary rocks of the Paleogene age. Ore-controlling zones are the fractured zones of the north-western direction, feathering the meridional fault. As a result of exploration, 26 ore bodies grouped into four ore zones were identified. Industrial uranium mineralisation was located at two levels (535 and 495 m) in the cementation zone of the deposit. The ores of the deposit represent brecciated, limonitised, often crushed granite-porphyrines (Belova and Tseitlin, 1959).

The underground workings at the deposit developed from the late 1940s until 1991. After they ceased, supergene oxidation of primary ores with uraninite and pyrite in the wet underground

environment of the mine yielded different secondary minerals, mainly sulfates, including gurzhiite. They fill the intermittent cavities of ore bodies, infiltrate breccias, and form veinlets, coatings and crusts on the surface of cracks and mine walls (Fig. 3).

Gurzhiite associates directly, and is sometimes intimately intergrown with, khademite. Other associated minerals include quartz and an unidentified fluoride of Al, most likely a F-analogue or a variety of nordstrandite $\text{Al}(\text{OH})_2\text{F}$. Other minerals found nearby, but not in close contact with gurzhiite include hydrokenoralstonite, natrozippite and schröckingerite.



Fig. 2. Bykogorskoe U deposit at Byk Mountain. Summer 2019. Photo: N. Operator.

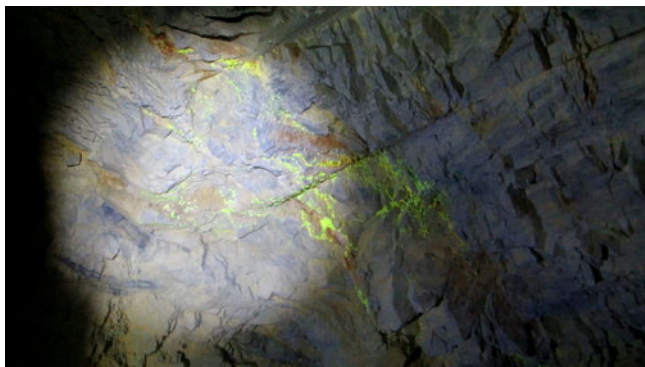


Fig. 3. Gurzhiite *in situ*. Field of view 2 × 1 m. Summer 2020. Photo: D. Tsebros.

General appearance and physical properties

Gurzhiite occurs as fine-grained aggregates forming veinlets up to 50 cm long in cracks of the brecciated rock. Gurzhiite aggregates are composed of small bladed crystals up to 0.1 mm across flattened on {001}. The new mineral is pale yellow in crystals and lemon yellow in aggregates (Fig. 4a). It is transparent with vitreous lustre and a white streak. Its tenacity is brittle and its fracture is irregular. Good cleavage on {001} is observed. Gurzhiite exhibits a bright yellow–green fluorescence under both longwave and shortwave UV radiation (Fig. 4b). Mohs hardness based on scratch tests is ~2. Density measured by flotation in heavy liquids

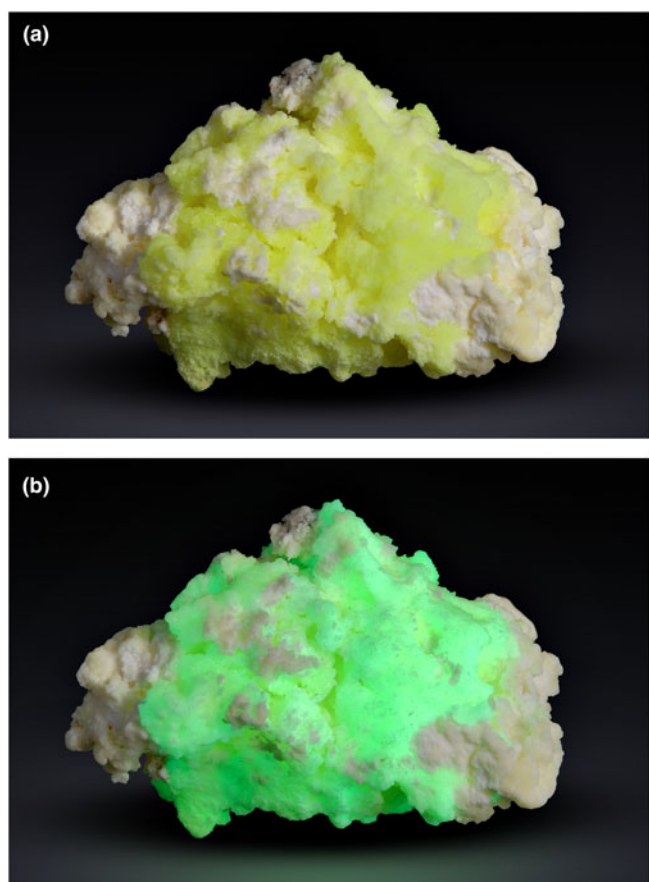


Fig. 4. (a) Lemon-yellow gurzhiite intermixed with white khademite; (b) same specimen under shortwave UV light. Specimen size: 1.4 × 0.8 cm. Specimen No.5756/1, photo: M. Milshina.

(bromoform + heptane) is 2.52(3) g/cm³; that calculated using the empirical formula and unit-cell volume obtained from single-crystal X-ray diffraction (XRD) data is 2.605 g/cm³. The lowered D_{meas} value as compared to D_{calc} may be due to porosity, inclusions of other minerals and/or partial dehydration of the mineral during measurement.

The mineral is colourless in transmitted light. It is biaxial (–) with $\alpha = 1.528(3)$, $\beta = 1.538(2)$ and $\gamma = 1.544(3)$ (589 nm). The estimated 2V angle based on the curve of the conoscopic figures is 80(10)°, the calculated 2V value is 75.1°. No dispersion or pleochroism were observed. The optical orientation cannot be determined due to the anhedral shape of the grains. The Gladstone–Dale compatibility index (Mandarino, 1981) calculated based on the empirical formula and unit-cell parameters from the single-crystal XRD data is $1 - (K_p/K_c) = -0.007$ (superior).

Spectroscopical studies

Infrared spectroscopy

In order to obtain an infrared (IR) absorption spectrum, a powdered gurzhiite sample was mixed with anhydrous KBr, pelletised, and analysed using an ALPHA FTIR spectrometer (Bruker Optics) in the range of 360–3800 cm⁻¹, at a resolution of 4 cm⁻¹. A total of 16 scans were collected. The IR spectrum of an analogous pellet of pure KBr was used as a reference. The assignment of absorption bands in the IR spectrum of gurzhiite (Fig. 5) was made in accordance with Čejka (1999), Nakamoto (2008, 2009), and Chukanov and Chervonnyi (2016). Bands in the range of 3200–3520 cm⁻¹ correspond to O–H stretching vibrations of H₂O molecules forming medium-strength hydrogen bonds (corresponding to O...O distances between ~2.7–3.1 Å; after Libowitzky (1999)). The bands at 2380 and 2550 cm⁻¹ correspond to O–H stretching vibrations of minor amounts of acid OH groups presumably formed due to the dynamic equilibrium $\text{H}_2\text{O} + \text{SO}_4^{2-} \leftrightarrow \text{OH}^- + \text{HSO}_4^-$ which is typical for high-hydrous sulfates (Chukanov and Chervonnyi, 2016). The bands at 1627 and 1675 cm⁻¹ are due to bending vibrations of non-equivalent H₂O molecules. The bands in the range of 1030–1200 cm⁻¹ are assigned to asymmetric stretching vibrations of SO_4^{2-} [the F_2 (ν_3) mode]. The band at 1015 cm⁻¹ corresponds to symmetric stretching vibrations of distorted SO_4^{2-} anions [the A_1 (ν_1) mode] and the one at 936 cm⁻¹ to antisymmetric stretching vibrations of the uranyl cation, UO_2^{2+} . The weak band at 858 cm⁻¹ is attributed to symmetric stretching vibrations of UO_2^{2+} . This band is forbidden in the IR spectrum of UO_2^{2+} with equivalent U–O bonds. Thus, the UO_2^{2+} group in gurzhiite is slightly distorted. This conclusion is in line with the structural data (see below). The bands in the range of 500–670 cm⁻¹ correspond to Al–O stretching and SO_4^{2-} bending [the F_2 (ν_4) mode] vibrations and resonance modes involving these vibrations. Finally, the bands at 440 and 467 cm⁻¹ are due to Al–F stretching and SO_4^{2-} bending [the E (ν_2) mode] vibrations, and/or resonance modes involving these vibrations. No bands of carbonate, nitrate, borate, and organic groups are observed in the IR spectrum of gurzhiite. The IR spectrum of gurzhiite is unique and does not have close analogues among IR spectra of other minerals.

Raman spectroscopy

The Raman spectrum of gurzhiite (Fig. 6) was obtained using a Horiba Labram HR Evolution spectrometer. This dispersive,

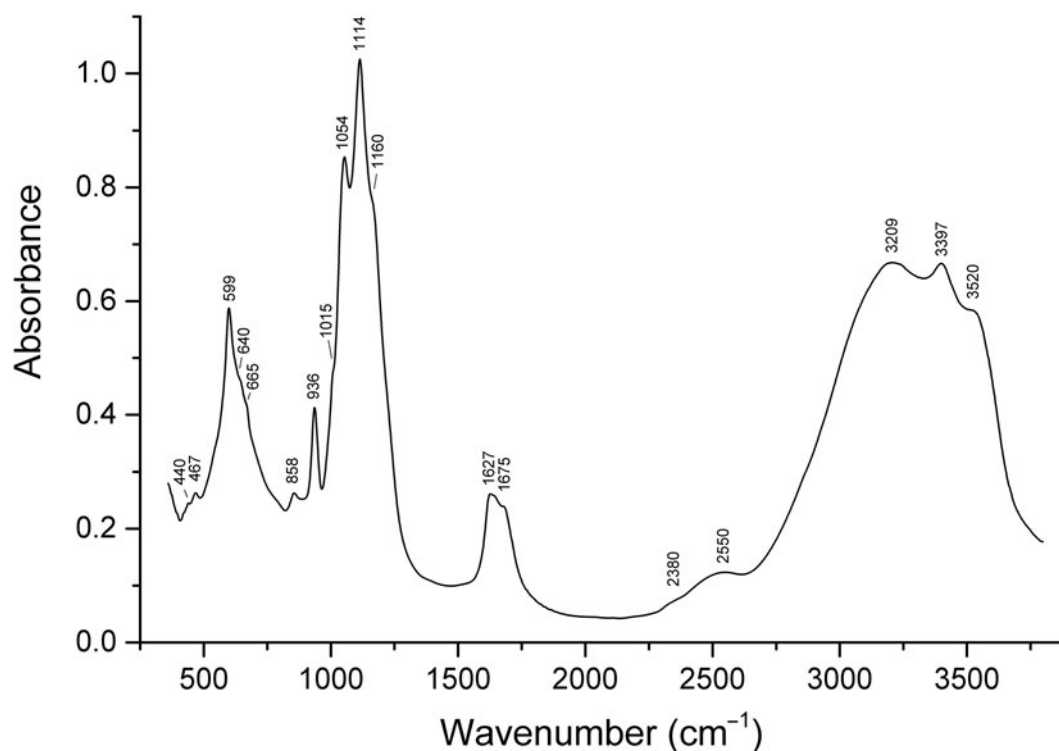


Fig. 5. Powder infrared absorption spectrum of gurzhiite.

edge-filter-based system is equipped with an Olympus BX 41 optical microscope, a diffraction grating with 600 grooves per millimetre, and a Peltier-cooled, Si-based charge-coupled device (CCD) detector. After careful tests with different lasers (473, 532 and 633 nm), the 633 nm He-Ne laser with the beam power of 1 mW at the sample surface was selected for spectra acquisition to minimise analytical artifacts. A Raman signal was collected in the range of 100–4000 cm^{-1} with a 50 \times objective with the system being operated in confocal mode, a beam diameter of $\sim 2.6 \mu\text{m}$ and lateral resolution of $\sim 5 \mu\text{m}$. No visual damage to the surface analysed was observed at these conditions after the excitation. Wavenumber calibration was done using the Rayleigh line and low-pressure Ne-lamp emissions. The wavenumber accuracy was $\sim 0.5 \text{ cm}^{-1}$, and the spectral resolution was $\sim 2 \text{ cm}^{-1}$. Band fitting was done after appropriate background correction, assuming combined Lorentzian–Gaussian band shapes using the Voigt function (*PeakFit*; Jandel Scientific Software, <http://www.sigmaplot.co.uk/products/peakfit/peakfit.php>). The assignment of the Raman bands is as follows. The bands in the range of 2900–3550 cm^{-1} correspond to O–H stretching vibrations. The weak bands at 1612 and 1677 cm^{-1} are due to bending vibrations of H_2O molecules. The bands in the 1020–1200 cm^{-1} range are attributed to asymmetric stretching vibrations of SO_4^{2-} [the $F_2(\nu_3)$ mode]. The bands at 991 and 1013 cm^{-1} correspond to symmetric stretching vibrations of two non-equivalent SO_4^{2-} anions [the $A_1(\nu_1)$ mode]. The weak band at 930 cm^{-1} is assigned to antisymmetric stretching vibrations of the uranyl cation. This band is forbidden in the Raman spectrum of UO_2^{2+} with equivalent U–O bonds, which is another proof of the slightly distorted character of the UO_2^{2+} group in gurzhiite. Bands at 833, 843 and 861 cm^{-1} are due to symmetric stretching vibrations of UO_2^{2+} , while those in the range of 500–650 cm^{-1} – to Al–O stretching and SO_4^{2-} bending

[the $F_2(\nu_4)$ mode] vibrations, as well as resonance modes involving these vibrations. Bands at 448 and 461 cm^{-1} correspond to Al–F stretching and SO_4^{2-} bending [the $E(\nu_2)$ mode] vibrations, as well as resonance modes involving these vibrations. The bands in the range of 160–230 cm^{-1} are attributed to UO_2^{2+} bending vibrations. Other Raman bands observed below 400 cm^{-1} correspond to lattice modes involving vibrations of the UO_2^{2+} and SO_4^{2-} groups as a whole (acoustic modes).

As seen below, there is only one site of U in the structure. Thus, only one band in the region of 830 to 870 cm^{-1} would be expected (as it takes place in the IR spectrum). However, three Raman bands are observed for gurzhiite in this range. The most convincing explanation would be Fermi resonance with overtones of the bands at 448 and 461 cm^{-1} provided that these bands correspond to Al–F stretching vibrations. Otherwise (in the case of bending vibrations of SO_4^{2-}) a positive anharmonic shift would be expected.

Chemical composition and chemical properties

Nine electron-microprobe analyses were carried out with a Cameca SX-100 electron microprobe in wavelength dispersive spectroscopy (WDS) mode with an accelerating voltage of 15 kV, a beam current on the specimen of 2 nA and a beam diameter of 8 μm . Peak counting times (CT) were 20 s for all elements; CT for each background was one-half of the peak time. The raw intensities were converted into concentrations using *X-PHI* (Merlet, 1994) matrix-correction software.

Hydrogen was analysed by gas chromatography of products of gurzhiite thermolysis at 1200 $^\circ\text{C}$ in oxygen with a CHN Vario Micro cube analyzer (Elementar GmbH, Germany).

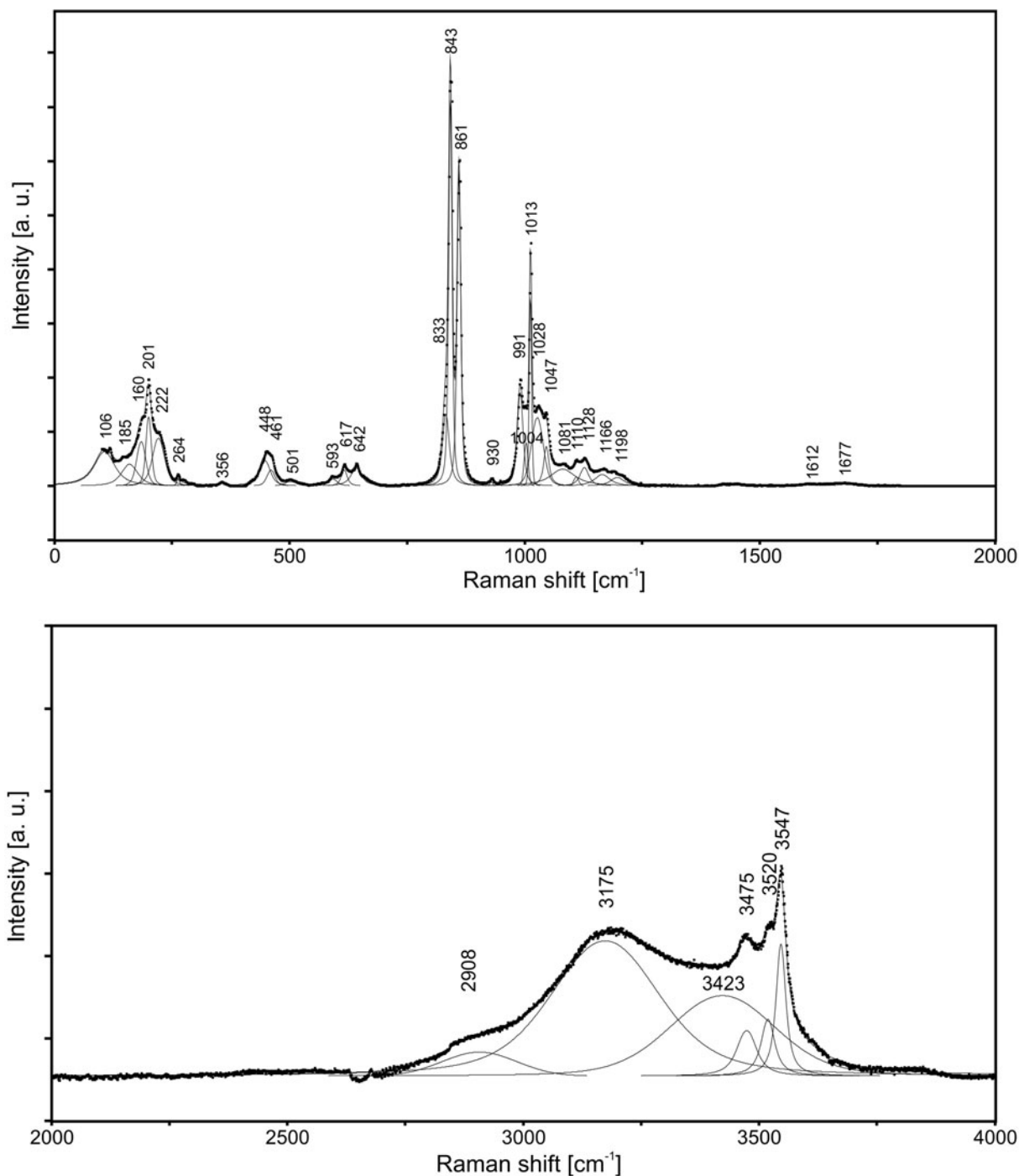


Fig. 6. Raman spectrum of gurzhiite excited by 633 nm laser: in the 100–1250 cm^{-1} region (*above*) and in the 2500–3600 cm^{-1} region (*below*). The measured spectrum is shown by dots. The curve matched to the dots is a result of spectral fit as a sum of individual Voigt peaks shown below the curve.

Analytical data and used standards are given in [Table 1](#). Contents of other elements with atomic numbers higher than that of beryllium are below detection limits. The empirical formula based on both WDS and CHN analyses calculated on the basis of 21 (O+F) apfu is $\text{Al}_{0.92}\text{Zn}_{0.05}\text{Fe}_{0.03}^{3+}\text{Na}_{0.03}\text{U}_{0.95}\text{S}_{2.00}\text{O}_{9.85}\text{F}_{0.99}\cdot 10.16\text{H}_2\text{O}$.

The ideal formula is $\text{Al}(\text{UO}_2)(\text{SO}_4)_2\text{F}\cdot 10\text{H}_2\text{O}$, which requires Al_2O_3 7.40, UO_3 41.53, SO_3 23.28, F 2.76, H_2O 26.19, $-\text{O}=\text{F}$ – 1.16, total 100 wt.%.

Gurzhiite is soluble in water and dissolves in hydrochloric and nitric acids without gas evolution.

X-ray diffraction data

The powder X-ray diffraction (XRD) data ([Table 2](#)) were obtained using a DRON-2.0 diffractometer with $\text{FeK}\alpha$ radiation, Mn-filter and quartz used as an internal standard. The unit-cell parameters refined from the powder data using *UNITCELL* software by Holland and Redfern (1997) are as follows: gurzhiite is triclinic, $P\bar{1}$, $a = 7.179(2)$, $b = 11.728(2)$, $c = 11.757(2)$ Å, $\alpha = 67.15(2)$, $\beta = 107.76(2)$, $\gamma = 89.97(2)^\circ$, $V = 860.7(2)$ Å³ and $Z = 2$.

The single-crystal X-ray diffraction data were collected using a Supernova Rigaku-Oxford Diffraction diffractometer equipped

Table 1. Chemical composition of gurzhiite (wt.%).

Constituent	Wt.%	Range	S.D.	Probe standard
Na ₂ O	0.12	0.00–0.20	0.14	Amelia albite
ZnO	0.63	0.29–1.31	0.37	Gahnite
Al ₂ O ₃	6.93	5.58–8.58	1.08	Sanidine
Fe ₂ O ₃	0.37	0.07–0.85	0.29	Almandine
SO ₃	23.76	22.39–24.85	0.96	SrSO ₄
UO ₃	40.35	39.46–41.99	0.76	UO ₂
F	2.79	2.30–3.10	0.27	Topaz
H ₂ O*	27.14			
–O=F	–1.17			
Total	100.92			

* 27.14 wt.% H₂O is calculated from 3.037 wt.% H determined by CHN-analysis.
S.D. – standard deviation

with micro-source MoK α radiation ($\lambda = 0.71073 \text{ \AA}$; 50 kV, 0.8 mA) and a Pilatus 200K Dectris detector. The sample-to-detector distance was set to 68 mm. The data were collected by 1569 frames over 27 runs; the exposure time was 60 seconds per frame for a total time equal to 26 hours and 17 minutes. The data were processed by *Crysalis Pro 41_64.113a* software (Rigaku Oxford Diffraction). The triclinic unit-cell parameters determined from single-crystal data are as follows: $a = 7.193(2)$, $b = 11.760(2)$, $c = 11.792(2) \text{ \AA}$, $\alpha = 67.20(3)^\circ$, $\beta = 107.76(3)^\circ$, $\gamma = 89.99(3)^\circ$ and $V = 867.7(4) \text{ \AA}^3$ ($Z = 2$).

The crystal structure of gurzhiite was solved from single-crystal X-ray data using the intrinsic phasing algorithm of the program *SHELXT* (Sheldrick, 2015) and refined to $R_{\text{obs}} = 0.0565$ and $wR_{\text{obs}} = 0.1098$ for 3236 reflections with $I > 3\sigma(I)$. The initially

Table 2. Powder X-ray diffraction data (d in \AA) of gurzhiite.

l_{meas}	l_{calc}^*	d_{meas}	d_{calc}	hkl
100	100	10.24	10.258	001
10	21	6.76	6.788	$\bar{1}01$
	21		6.788	100
2	13	5.83	5.833	021
14	23	5.40	5.419	$\bar{1}\bar{1}1$
	20		5.418	$\bar{1}10$
54	34	5.11	5.129	002
	6		5.110	111
	6		5.110	$\bar{1}\bar{1}2$
6	9	4.941	4.957	101
	8		4.957	$\bar{1}02$
2	7	4.803	4.815	022
2	6	4.102	4.119	$0\bar{2}1$
5	8	4.053	4.067	$\bar{1}\bar{1}2$
	7		4.067	$\bar{1}\bar{1}1$
8	15	3.618	3.630	023
11	8	3.405	3.410	$\bar{2}11$
	7		3.410	$\bar{2}\bar{1}1$
	6		3.369	210
	5		3.369	$\bar{2}\bar{1}2$
7	8	3.348	3.360	130
	8		3.359	$\bar{1}31$
3	7	3.134	3.142	$\bar{1}33$
	6		3.142	132
11	8	3.065	3.074	$\bar{1}\bar{1}3$
	7		3.073	$\bar{1}\bar{1}2$
	5		2.916	042
4	8	2.897	2.904	041
5	6	2.790	2.799	024
4	5	2.583	2.591	$\bar{2}33$

*For the calculated pattern only reflections with intensities ≥ 5 are given
The strongest reflections are given in bold

Table 3. Summary of data collection conditions and refinement parameters for gurzhiite.

Crystal data	
Chemical formula sum	AlFUS ₂ O ₂₀
Crystal size (mm)	0.080 × 0.060 × 0.010
Crystal system	Triclinic
Space group	$P\bar{1}$
Unit-cell parameters: a, b, c (\AA)	7.193(2), 11.760(2), 11.792(2)
α, β, γ ($^\circ$)	67.20(3), 107.76(3), 89.99(3)
Unit-cell volume (\AA^3)	867.7(4)
Z	2
Calculated density (g/cm^3)	2.557 (for the formula from the structure without H atoms)
Temperature (K)	293
Limiting Miller indices	$h = -10 \rightarrow 10$ $k = -17 \rightarrow 17$ $l = -17 \rightarrow 17$
Data collection	
Diffractometer	Rigaku SuperNova with Pilatus 200K
Radiation, wavelength (\AA)	MoK α , 0.71073 (50 kV, 30 mA)
θ range for data collection ($^\circ$)	1.90–31.90
Axis, frame width ($^\circ$), time per frame (s)	ω , 1.0, 60
Total reflections collected	17983
Unique reflections	5457
Unique observed reflections, criterion	3236, [$I > 3\sigma(I)$]
Absorption coefficient (mm^{-1}), type	9.75; multi-scan
$T_{\text{min}}/T_{\text{max}}$	0.679/1
Data completeness to θ_{max} ($\%$), R_{int}	91.00, 0.077
Refinement	
Structure refinement	Full-matrix least-squares on F
No. of param., restraints, constraints	205, 2, 1
R, wR (obs)	0.0562, 0.1093
R, wR (all)	0.1246, 0.1261
GOF obs/all	1.74, 1.98
Weighting scheme, weights	$\sigma, w = 1/(\sigma^2(I) + 0.0004I^2)$
Largest diff. peak and hole ($e^-/\text{\AA}^3$)	4.15, -3.51
Twin matrix; $T_{w_{\text{vol}1}}/T_{w_{\text{vol}2}}$	$\begin{pmatrix} 1 & 0 & 0 \\ 0 & -1 & 0 \\ -1 & 0 & -1 \end{pmatrix}; 0.469(5)/0.531(5)$

determined monoclinic cell with $a = 20.683$, $b = 7.193$, $c = 11.760 \text{ \AA}$, $\beta = 97.290(4)^\circ$ and $V = 2 \times 867.7 \text{ \AA}^3$ corresponds to I -centred symmetry. However, based on the metrics and space-group tests procedures implemented in *Jana2020*, which is the successor of the *Jana2006* program (Petříček *et al.*, 2014), we concluded that the crystal studied is twinned and its true symmetry is triclinic, as indicated above. The monoclinic pseudo-cell with doubled volume results from the twinning due to metric merohedry (diffraction type I; Petříček *et al.*, 2016). The twinned super-cell can be obtained *via* a mirror in (101), leading to a monoclinic I -centred cell mentioned above. No H atoms could have been successfully localised from the difference-Fourier maps. In line with the previously refined structure of straßmannite (Kampf *et al.*, 2019), we have initially assigned the cation–anion distance of $\sim 1.79 \text{ \AA}$ in the Al-centred tetrahedron, which is too short for Al–O or Al–O_{H₂O}, to the Al–F bond. The results of the chemical study indicate that there should be nearly stoichiometric content of F (1 F apfu) which is in line with the structure refinement, taking into account that O9 is to be fully occupied by F (therefore designated as F9 further on). The rest of the bonds around Al sites are also somewhat shorter

Table 4. Atom coordinates, isotropic and equivalent displacement parameters (in Å) for gurzhiite.

Atom	<i>x/a</i>	<i>y/b</i>	<i>z/c</i>	<i>U</i> _{iso} */ <i>U</i> _{eq}
U1	-0.12647(12)	-0.74999(18)	0.5003(2)	0.0291(3)
S1	0.2545(13)	-0.9989(9)	0.5974(11)	0.027(4)
S2	0.1657(15)	-0.5002(10)	0.4002(9)	0.032(4)
Al1	1	-1/2	1	0.034(7)
Al2	-1/2	0	0	0.035(7)
O1	-0.045(4)	-0.821(2)	0.6733(7)	0.0257(9)*
O2	-0.215(4)	-0.679(2)	0.3278(7)	0.0257(9)*
O3	0.231(4)	-1.068(2)	0.510(3)	0.033(8)
O4	0.848(3)	-0.6267(18)	0.979(2)	0.036(9)
O5	0.331(3)	-0.526(2)	0.349(2)	0.032(7)
O6	0.180(3)	-1.068(2)	0.703(2)	0.030(6)*
O7	0.447(3)	-0.985(2)	0.652(2)	0.029(7)
O8	0.131(4)	-0.872(2)	0.507(3)	0.051(7)
F9	-0.398(3)	-0.1243(18)	-0.024(2)	0.045(7)
O10	0.132(3)	-0.6230(19)	0.4853(19)	0.027(4)*
O11	-0.503(4)	-0.116(2)	0.162(2)	0.034(8)
O12	0.248(4)	-0.434(2)	0.483(3)	0.029(7)
O13	-0.018(4)	-0.436(2)	0.298(3)	0.048(7)
O14	0.820(4)	-0.460(2)	1.069(3)	0.039(10)
O15	0.831(5)	-0.391(2)	0.828(2)	0.048(11)
O16	-0.020(4)	-0.8199(19)	0.9343(18)	0.030(8)
O17	-0.759(4)	-0.038(2)	-0.081(3)	0.042(10)
O18	0.449(4)	-0.313(3)	0.930(3)	0.063(14)
O19	-0.433(4)	-0.354(3)	0.239(2)	0.045(11)
O20	-0.176(4)	-0.153(3)	0.759(3)	0.055(13)
O21	-0.4737(12)	-0.7490(13)	0.4794(12)	0.033(2)*

than the regular Al–O bonds. Thus, F may be distributed among those O sites. Nevertheless, the attempts to refine all of the ligands as mixed O/F sites did not improve the fit. Therefore the single F site was kept for the final model. Final refinement using anisotropic displacement parameters for the majority of remaining atoms in the structure converged with reasonable values of agreement (Table 3). The final fit also required restrictions on the U–O bond-lengths in uranyl, hence U–O1/O2 distances were restrained to 1.800(5) Å, as the refined values were slightly unrealistically short (~1.73 Å). We account for that as due to a complete overlap of the measured intensities of reflections due to twinning. Atom coordinates and isotropic/equivalent displacement parameters are given in Table 4 (anisotropic ones are listed in the crystallographic information file). Selected interatomic distances are listed in Table 5 and a bond-valence analysis, done following the procedure of Brown (2002) using bond-valence parameters by

Table 5. Selected interatomic distances (in Å) in the crystal structure of gurzhiite.

Al1–O4	1.90(2)	U1–O1	1.776(8)	S1–O3	1.51(4)
Al1–O4 ⁱⁱⁱ	1.90(2)	U1–O2	1.770(7)	S1–O6	1.46(3)
Al1–O14	1.87(4)	U1–O3 ⁱ	2.30(3)	S1–O7	1.38(2)
Al1–O14 ⁱⁱⁱ	1.87(4)	U1–O8	2.31(3)	S1–O8	1.53(2)
Al1–O15	1.928(19)	U1–O10	2.39(2)	<S1–O>	1.47
Al1–O15 ⁱⁱⁱ	1.928(19)	U1–O12 ⁱⁱ	2.43(3)		
<Al1–O>	1.90	U1–O21	2.434(8)	S2–O5	1.56(3)
		<U1–O _{ur} >	1.77	S2–O10	1.48(2)
Al2–F9	1.79(3)	<U1–O _{eq} >	2.37	S2–O12	1.46(4)
Al2–F9 ^{iv}	1.79(3)			S2–O13	1.45(2)
Al2–O11	1.88(2)			<S2–O>	1.49
Al2–O11 ^{iv}	1.88(2)				
Al2–O17	1.96(3)				
Al2–O17 ^{iv}	1.96(3)				
<Al2–O>	1.88				

Symmetry codes: (i) $-x, -y-2, -z+1$; (ii) $-x, -y-1, -z+1$; (iii) $-x+2, -y-1, -z+2$; (iv) $-x-1, -y, -z$.

Gagné and Hawthorne (2015) and Brown and Altermatt (1985) (for the Al–F bond) is in Table 6. The crystallographic information file has been deposited with the Principal Editor of *Mineralogical Magazine* and is available as Supplementary material (see below).

Description of the crystal structure

The structure of gurzhiite contains a single U site, two S sites, two Al sites, one F and twenty O sites (Fig. 7). The U site is linked to seven O atoms forming a squat UO₇ pentagonal bipyramid, where two short (~1.8 Å in length) apical bonds constitute the uranyl ion (Table 5). This is the most typical coordination for hexavalent uranium in the form of the uranyl ion, UO₂²⁺, particularly in uranyl sulfates. The UO₇ bipyramids share four of their equatorial vertices (O3, O8, O10 and O12) with tetrahedrally coordinated sulfur atoms, forming thus four monodentate UO₇–SO₄ linkages. The remaining unshared equatorial vertex O21 of the uranyl bipyramid (Table 6) is occupied by the O atom of the H₂O molecule forming hydrogen bonds with free vertices of the SO₄ tetrahedra, the same as takes place in strassmannite (Kampf *et al.*, 2019). The UO₇ and SO₄ polyhedra with attached water molecules form infinite [(UO₂)(SO₄)₂(H₂O)]²⁻ chains running along [010]. Between the chains, there are two independent Al-based octahedra, Al1(H₂O)₆ and Al2F₂(H₂O)₄. They are linked to the chains on either side *via* a complex network of assumed hydrogen bonds.

Chains found in gurzhiite (Fig. 8) are of the same topology as chains in the uranyl sulfates bobcookite, Na(H₂O)₂Al(H₂O)₆[(UO₂)₂(SO₄)₄(H₂O)₂]·8H₂O (Kampf *et al.*, 2015a), oppenheimerite, Na₂(H₂O)₂[(UO₂)(SO₄)₂(H₂O)] (Kampf *et al.*, 2015b), svornostite, K₂Mg[(UO₂)(SO₄)₂]₂·8H₂O (Plášil *et al.*, 2015), rietveldite, Fe(UO₂)(SO₄)₂·5H₂O (Kampf *et al.*, 2017), old-site, K₂Fe[(UO₂)(SO₄)₂]₂·8H₂O (Plášil *et al.*, 2021), synthetic K₂[(UO₂)(SO₄)₂(H₂O)](H₂O) (Ling *et al.*, 2010), and synthetic Mn(UO₂)(SO₄)₂(H₂O)₅ (Tabachenko *et al.*, 1979).

Discussion

Chemically, gurzhiite, Al(UO₂)(SO₄)₂F·10H₂O (*Z* = 2), is very similar to strassmannite, Al(UO₂)(SO₄)₂F·16H₂O (*Z* = 4) (Kampf *et al.*, 2019), being the lower hydrate of the latter. Strassmannite was also found in Mine #2 of the Bykogorskoe deposit and reliably identified by semi-quantitative energy-dispersive spectroscopy analysis (Al, U, S and F with approximate ratio 1:1:2:1) and single-crystal XRD (monoclinic unit-cell with *a* = 11.011(2), *b* = 8.3103(15), *c* = 26.635(10) Å, β = 97.48(2)°, *V* = 2417(1) Å³). Thus, one can suppose that gurzhiite may form *via* dehydration of strassmannite. However, this transformation would be accompanied by a significant structural reorganisation as the strassmannite structure is based upon uranyl sulfate sheets, while gurzhiite is based upon uranyl sulfate chains. Usually, the mechanism/trend in hydrated oxysalts is that the structures of higher hydrates are based upon the clusters or chains (due to the depolymerising action of H₂O), while the lower hydrates have sheet structures (c.f. Hawthorne and Sokolova, 2012). Therefore, we do not think that gurzhiite at the Bykogorskoe deposit formed from strassmannite. Noteworthy is that gurzhiite and strassmannite have been found at different levels of the Mine #2 of the Bykogorskoe deposit, i.e. at a substantial distance from each other, so they probably formed in a different underground environment (different humidity, oxidising conditions and pH).

Table 6. Bond-valence analysis (values given in the valence units, vu) of the crystal structure of gurzhiite.

	U1	Al1	Al2	S1	S2	Sum	Assignment	nH	Sum ⁺
O1	1.77					1.77	O ⁺ H	1	1.97
O2	1.79					1.79	O ⁺ H	1	1.99
O3	0.58			1.36		1.95	O	0	
O4		0.51×2↓				0.51	H ₂ O	0	2.11
O5					1.20	1.20	O ⁺ H	4	2.04
O6				1.55		1.55	O ⁺ H	2	1.95
O7				1.89		1.89	O ⁺ H	1	2.09
O8	0.57			1.30		1.87	O ⁺ H	1	2.07
F9			0.52×2↓			0.52	F	2	0.92
O10	0.48				1.47	1.95	O	0	
O11			0.53×2↓			0.53	H ₂ O	0	2.13
O12	0.44				1.55	1.99	O	0	
O13					1.59	1.59	O ⁺ H	2	1.99
O14		0.55×2↓				0.55	H ₂ O	0	2.15
O15		0.47×2↓				0.47	H ₂ O	0	2.07
O16						0.00	H ₂ O	+2×0.2	1.60
O17			0.43×2↓			0.43	H ₂ O	0	2.03
O18						0.00	H ₂ O	+2×0.2	1.60
O19						0.00	H ₂ O	+2×0.2	1.60
O20						0.00	H ₂ O	+2×0.2	1.60
O21	0.44					0.44	H ₂ O	0	2.04
Sum	6.09	3.04	2.96	6.10	5.81				

Notes: Sum⁺ – the sum of the BV including assumed H bonds (considering the theoretical H-bond strengths of 0.8 or 0.2 vu for O atoms belonging to H₂O molecules being donors of H bonds and O atoms – acceptors of H bonds, respectively, after Brown, 2002); nH – theoretical number of the weak H bonds that could be accepted by the O atom; O⁺H – a character of the O atom which, however, has to accept at least one weak H bond to meet its bond-valence requirements.

From the point of the view of the structural complexity (*sensu* Krivovichev, 2013), straßmannite possesses a complex structure, with 699 bits/unit-cell (Gurzhiy and Plášil, 2019). Gurzhiite is less complex, having 482.43 bits/unit-cell [calculated by the program *TOPOS* including theoretical/dummy H atoms (Blatov *et al.*, 2014)], which is in line with the lower total atomic content of the unit cell as the structure is smaller. Notably, gurzhiite has a

greater complexity per atom, 5.48 bits/atom, than 5.07 bits/atom in straßmannite.

Another interesting point is the fluorine content in gurzhiite. Fluorine, in general, is a very rare component of uranyl oxysalts. Gurzhiite is only the second (after straßmannite) uranyl sulfate from 57 and only the eighth (after albrechtschraufite, arsenuranospathite, chistyakovaite, nollmotzite,

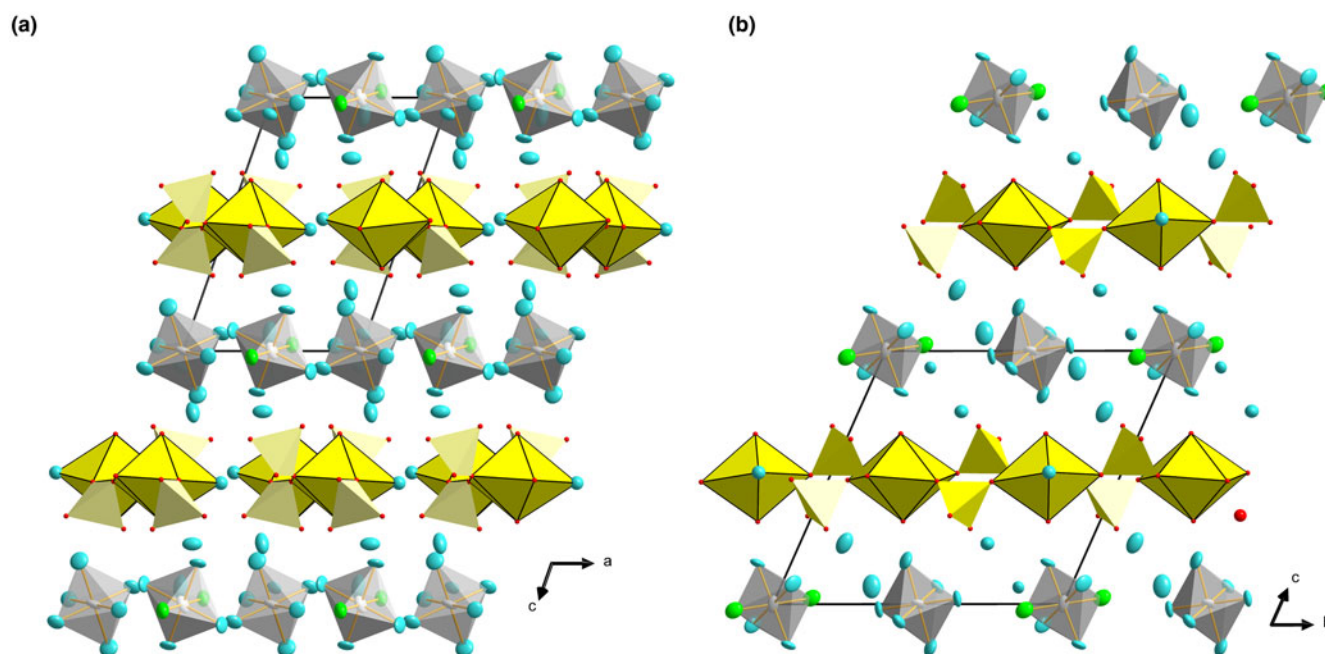


Fig. 7. Crystal structure of gurzhiite. (a) View down **b** and (b) viewed down **a** (perpendicular to the infinite UO₇–SO₄ chains). UO₇ polyhedra yellow with black edges, SO₄ tetrahedra light yellow without emphasised edges, Al-octahedra grey, O atoms of the H₂O molecules in aqua, otherwise purely O atoms are in red and F in green; unit-cell edges outlined in black solid lines.

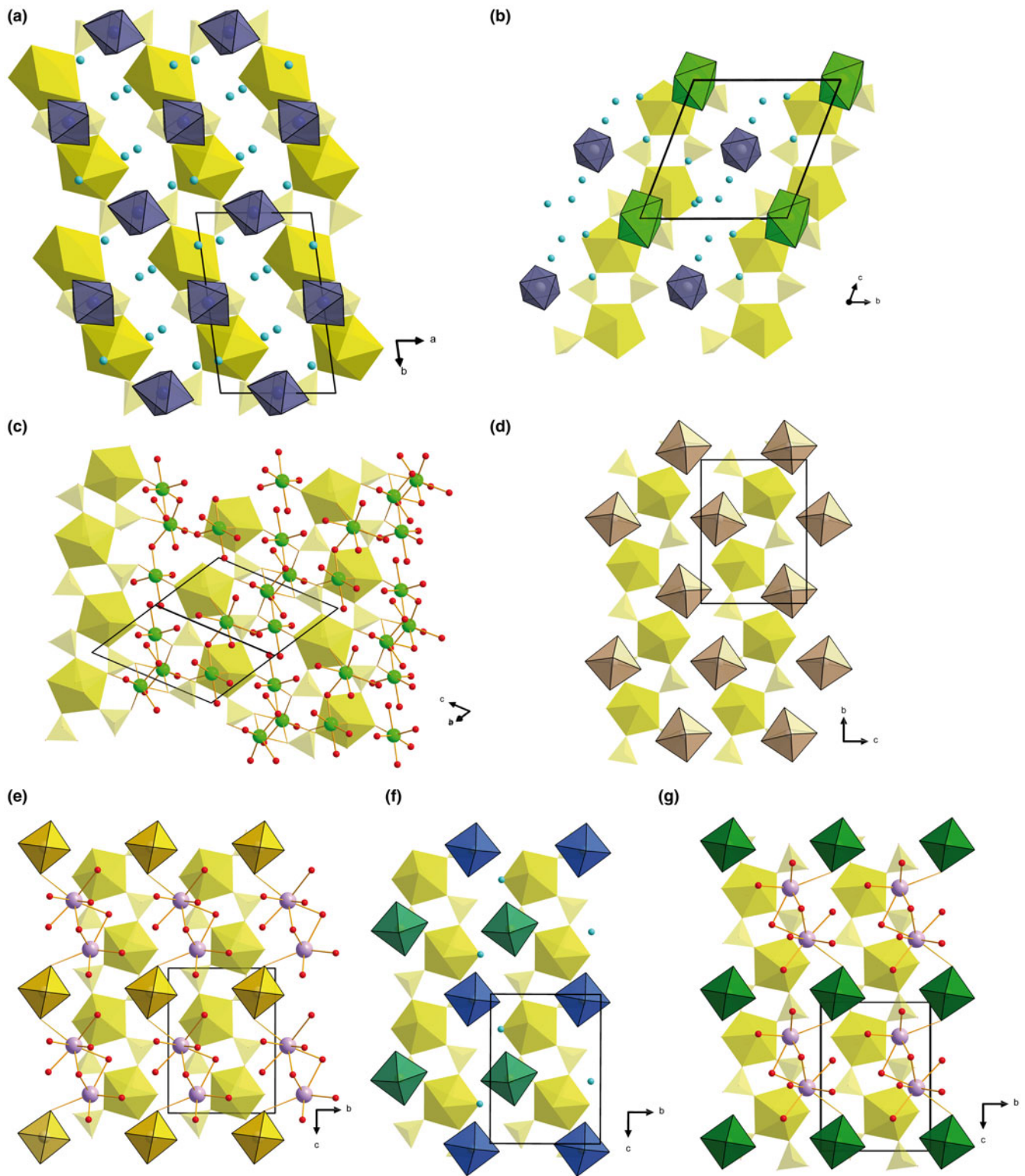


Fig. 8. Crystal structures of (a) gurzhiite and related uranyl sulfates (b–g): (b) bobcookite (Na octahedra in green and Al octahedra in blue–grey); (c) oppenheimerite (Na as green balls); (d) synthetic $\text{Mn}(\text{UO}_2)(\text{SO}_4)_2(\text{H}_2\text{O})_5$; (e) svornostite (Mg in gold and K lavender); (f) rietveldite (Fe octahedra green, mixed Fe–Zn octahedra in blue colour); (g) oldsite (Fe in green and K lavender). O atoms of the isolated H_2O groups are in azure-blue, other O atoms are in red; H atoms were omitted for clarity. Unit-cell edges are outlined by black lines.

schröckingerite, straßmannite and uranospathe) uranyl oxy-salt to contain F as a species-defining element. Most of these minerals also have essential Al. Earlier, Kampf *et al.* (2019) noted the well-known affinity of Al for F and suggested that there were Al fluoride complexes in the solutions from which straßmannite and other Al–U–F-bearing minerals formed. In the case of gurzhiite, such a precursor could be an unidentified fluoride of Al, most likely a F-analogue or a variety of nordstrandite Al(OH)₂F found in close association with the former.

Supplementary material. To view supplementary material for this article, please visit <https://doi.org/10.1180/mgm.2022.34>

Acknowledgements. We thank reviewers Sergey Krivovichev, Travis Olds and Nicolas Meisser, Structural Editor Peter Leverett and Principal Editor Stuart Mills for valuable comments. This study was funded by the Czech Science Foundation (GACR 20-11949S to J.P.) and by OP VVV project (Geobarr CZ.02.1.01/0.0/0.0/16_026/0008459 to R.Š.). The IR spectroscopy study, interpretation of the Raman spectrum, and analysis of H₂O were performed in accordance with the state task of the Russian Federation, state registration No. AAAA-A19-119092390076-7.

Competing interests. The authors declare none.

References

- Belova L.N. and Tseitlin S.G. (1959) *Mineralogical Features of Oxidation Zones of Beshtau and Byk Deposits*. Geolfond IGEM RAN, Moscow, 34 pp. [in Russian].
- Blatov V.A., Shevchenko A.P. and Proserpio D.M. (2014) Applied topological analysis of crystal structures with the program package ToposPro. *Crystal Growth & Design*, **14**, 3576–3586.
- Brown I.D. (2002) *The Chemical Bond in Inorganic Chemistry: The Bond Valence Model*. Oxford University Press, Oxford, UK.
- Brown I.D. and Altermatt D. (1985) Bond-valence parameters obtained from a systematic analysis of the inorganic crystal structure database. *Acta Crystallographica*, **B41**, 244–248.
- Čejka, J. (1999) Infrared spectroscopy and thermal analysis of the uranyl minerals. Pp. 521–622 in: *Uranium: Mineralogy, Geochemistry, and the Environment* (P.C. Burns and R.J. Finch, editors). **38**. Mineralogical Society of America, Washington DC, USA.
- Chukanov N.V. and Chervonnyi A.D. (2016) *Infrared Spectroscopy of Minerals and Related Compounds*. Springer, Cham–Heidelberg–Dordrecht–New York–London, 1109 pp.
- Gagné O.C. and Hawthorne F.C. (2015) Comprehensive derivation of bond-valence parameters for ion pairs involving oxygen. *Acta Crystallographica*, **B71**, 562–578.
- Gurzhiy V.V. and Plášil J. (2019) Structural complexity of natural uranyl sulfates. *Acta Crystallographica*, **B75**, 39–48.
- Gurzhiy V.V., Tyumentseva O.S., Krivovichev S.V., Krivovichev V.G. and Tananaev I.G. (2016) Mixed uranyl sulfate-selenates: variable composition and crystal structures. *Crystal Growth and Design*, **16**, 4482–4492.
- Gurzhiy V.V., Krzhizhanovskaya M.G., Izatulina A.R., Sigmon G.E., Krivovichev S.V. and Burns P.C. (2018) Structure refinement and thermal stability studies of the uranyl carbonate mineral andersonite, Na₂Ca[(UO₂)(CO₃)₃]₃·(5+x)H₂O. *Minerals*, **8**, 586.
- Gurzhiy V.V., Kuporev I.V., Kovrugin V.N., Murashko M.N., Kasatkin A.V. and Plášil J. (2019) Crystal chemistry and structural complexity of natural and synthetic uranyl selenites. *Crystals*, **9**, 639.
- Gurzhiy V.V., Izatulina A.R., Krzhizhanovskaya M.G., Murashko M.N., Spiridonova D.V., Shilovskikh V.V. and Krivovichev S.V. (2020) Thermal behavior of uranyl selenite minerals derriksite and demesmaekerite. *Journal of Geosciences*, **65**, 249–259.
- Gurzhiy V.V., Kalashnikova S.A., Kuporev I.V. and Plášil J. (2021) Crystal chemistry and structural complexity of the uranyl carbonate minerals and synthetic compounds. *Crystals*, **11**, 704.
- Hawthorne F.C. and Sokolova, E. (2012) The role of H₂O in controlling bond topology: I. The [6]Mg(SO₄)(H₂O)_n (n = 0–11) structures. *Zeitschrift für Kristallographie*, **227**, 594–603.
- Holland T.J.B. and Redfern S.A.T. (1997) Unit cell refinement from powder diffraction data: the use of regression diagnostics. *Mineralogical Magazine*, **61**, 65–77.
- Kampf A.R., Plášil J., Kasatkin A.V. and Marty J. (2015a) Bobcookite, NaAl(UO₂)₂(SO₄)₄(H₂O)₁₈, and wetherillite, Na₂Mg(UO₂)₂(SO₄)₄·18H₂O, two new uranyl sulfate minerals from the Blue Lizard mine, San Juan County, Utah, USA. *Mineralogical Magazine*, **79**, 695–714.
- Kampf A.R., Plášil J., Kasatkin A.V., Marty J. and Čejka J. (2015b) Fermitte, Na₄(UO₂)(SO₄)₃·3H₂O and oppenheimerite, Na₂(UO₂)(SO₄)₂·3H₂O, two new uranyl sulfate minerals from the Blue Lizard mine, San Juan County, Utah, USA. *Mineralogical Magazine*, **79**, 1123–1142.
- Kampf A.R., Sejkora J., Witzke T., Plášil J., Čejka J., Nash B.P. and Marty J. (2017) Rietveldite, Fe(UO₂)(SO₄)₂(H₂O)₅, a new uranyl sulfate mineral from Giveaway-Simplot mine (Utah, USA), Willi Agatz mine (Saxony, Germany) and Jáchymov (Czech Republic). *Journal of Geosciences*, **62**, 107–120.
- Kampf A.R., Plášil J., Kasatkin A.V., Nash B.P. and Marty J. (2019) Magnesioleydetite and straßmannite, two new uranyl sulfate minerals with sheet structures from Red Canyon, Utah. *Mineralogical Magazine*, **83**, 349–360.
- Kasatkin A.V., Plášil J., Chukanov N.V., Škoda R., Nestola F., Agakhanov A.A. and Belakovskiy D.I. (2022) Gurzhiite, IMA 2021-086. CNMNC Newsletter No. 65. *Mineralogical Magazine*, **86**, 354–358, <https://doi.org/10.1180/mgm.2022.14>
- Krivovichev S.V. (2013) Structural complexity of minerals: information storage and processing in the mineral world. *Mineralogical Magazine*, **77**, 275–326.
- Krivovichev S.V. and Plášil J. (2013) Mineralogy and crystallography of uranium. Pp. 15–119 in: *Uranium: from Cradle to Grave* (P.C. Burns and G.E. Sigmon, editors). MAC Short Courses, Vol. 43. Mineralogical Association of Canada, Québec, Canada.
- Libowitzky E. (1999) Correlation of O–H stretching frequencies and O–H...O hydrogen bond lengths in minerals. *Monatshefte für Chemie*, **130**, 1047–1059.
- Ling J., Sigmon G.E., Ward M., Roback N. and Burns P.C. (2010) Syntheses, structures, and IR spectroscopic characterization of new uranyl sulfate/selenate 1D-chain, 2D-sheet and 3D framework. *Zeitschrift für Kristallographie*, **225**, 230–239.
- Mandarino J.A. (1981) The Gladstone–Dale relationship. IV. The compatibility concept and its application. *The Canadian Mineralogist*, **19**, 441–450.
- Merlet C. (1994) An Accurate Computer Correction Program for Quantitative Electron Probe Microanalysis. *Microchimica Acta*, **114/115**, 363–376.
- Nakamoto K. (2008) *Infrared and Raman Spectra of Inorganic and Coordination Compounds, Theory and Applications in Inorganic Chemistry*. John Wiley and Sons, New York.
- Nakamoto K. (2009) *Infrared and Raman Spectra of Inorganic and Coordination Compounds, Part B, Applications in Coordination, Organometallic, and Bioinorganic Chemistry*. John Wiley and Sons, Hoboken, New York.
- Petríček V., Dušek M. and Palatinus L. (2014) Crystallographic computing system Jana 2006: general features. *Zeitschrift für Kristallographie*, **229**, 345–352.
- Petríček V., Dušek M. and Plášil J. (2016) Crystallographic computing system Jana2006: Solution and refinement of twinned structures. *Zeitschrift für Kristallographie*, **231**, 583–599.
- Plášil J. (2014) Oxidation-hydration weathering of uraninite: the current state-of-knowledge. *Journal of Geosciences*, **59**, 99–114.
- Plášil J., Hloušek J., Kasatkin A.V., Novák M., Čejka J. and Lapčák L. (2015) Svornostite, K₂Mg[(UO₂)(SO₄)₂]₂·8H₂O, a new uranyl sulfate mineral from Jáchymov, Czech Republic. *Journal of Geosciences*, **60**, 113–121.
- Plášil J., Kampf A.R., Ma C. and Desor J. (2021) Oldsite, IMA 2021-075. CNMNC Newsletter 64. *Mineralogical Magazine*, **85**, <https://doi.org/10.1180/mgm.2021.93>
- Sheldrick G.M. (2015) SHELXT – Integrated space-group and crystal-structure determination. *Acta Crystallographica*, **A71**, 3–8.
- Tabachenko V.V., Serezhkin V.I., Serezhkina L.B. and Kovba L.M. (1979) Crystal structure of manganese sulfatouranilate MnUO₂(SO₄)₂(H₂O)₅. *Koordinatsionnaya Khimiya*, **5**, 1563–1568.